

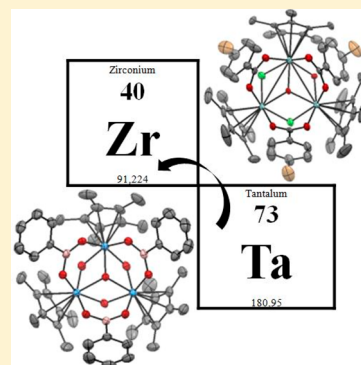
Synthesis of Carboxylate Cp*Zr(IV) Species: Toward the Formation of Novel Metallocavitands

Maxime Daigle,^{†,‡,§} Wenhua Bi,[†] Marc-André Légaré,^{†,§} Jean-François Morin,^{*,†,‡} and Frédéric-Georges Fontaine^{*,†,§}

[†]Département de Chimie, [‡]Centre de Recherche sur les Matériaux Avancés (CERMA), and [§]Centre de Catalyse et Chimie Verte (C3V), Université Laval, 1045 Avenue de la Médecine, Québec, Québec, Canada, G1V 0A6

Supporting Information

ABSTRACT: With the intent of generating metallocavitands isostructural to species $[(\text{CpZr})_3(\mu^3\text{-O})(\mu^2\text{-OH})_3(\kappa_{\text{O,O}}\mu^2\text{-O}_2\text{C(R)})_3]^+$, the reaction of Cp^*ZrCl_2 and Cp^*ZrCl_3 with phenylcarboxylic acids was carried out. Depending on the reaction conditions, five new complexes were obtained, which consisted of $\text{Cp}^*\text{ZrCl}(\kappa^2\text{-OOCPh})$ (1), $(\text{Cp}^*\text{ZrCl}(\kappa^2\text{-OOCPh}))_2(\mu\text{-}\kappa^2\text{-OOCPh})_2$ (2), $[(\text{Cp}^*\text{Zr}(\kappa^2\text{-OOCPh}))_2(\mu\text{-}\kappa^2\text{-OOCPh})_2(\mu^2\text{-OH})_2]\cdot\text{Et}_2\text{O}$ (3·Et₂O), $[(\text{Cp}^*\text{ZrCl}_2)(\mu\text{-Cl})(\mu\text{-OH})(\mu\text{-O}_2\text{CC}_6\text{H}_5)[\text{Cp}^*\text{Zr}]]_2(\mu\text{-O}_2\text{CC}_6\text{H}_5)_2$ (4), and $[\text{Cp}^*\text{ZrCl}_4][(\text{Cp}^*\text{Zr})_3(\kappa_2\text{-OOC}(\text{C}_6\text{H}_4\text{Br})_3(\mu_3\text{-O})(\mu_2\text{-Cl})_2(\mu_2\text{-OH}))][5]^+[\text{Cp}^*\text{ZrCl}_4]^-$. The structural characterization of the five complexes was carried out. Species 3·Et₂O exhibits host–guest properties where the diethyl ether molecule is included in a cavity formed by two carboxylate moieties. The secondary interactions between the cavity and the diethyl ether molecule affect the structural parameters of the complex, as demonstrated by the comparison of the density functional theory models for 3 and 3·Et₂O. Species 5 was shown to be isostructural to the $[(\text{CpZr})_3(\mu^3\text{-O})(\mu^2\text{-OH})_3(\kappa_{\text{O,O}}\mu^2\text{-O}_2\text{C(R)})_3]^+$ metallocavitands.

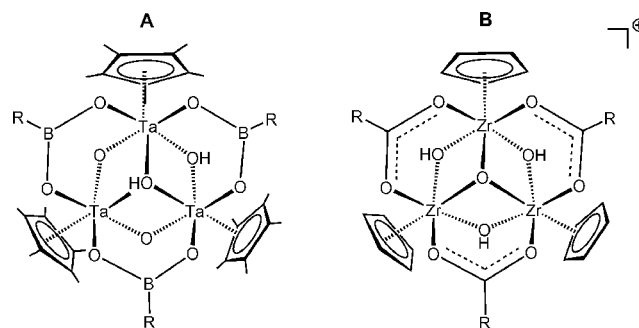


INTRODUCTION

Since the discovery of supramolecular assemblies in biological systems, there has been an ongoing interest in the design of supramolecular devices for various purposes, notably for molecular recognition¹ and catalysis.² Although several supramolecular architectures have been explored, cavitands are a class of molecules of particular interest. These species act as molecular cavities that can host an array of guest molecules according to shape and/or specific weak interactions, such as hydrogen bonding and π – π interactions. The most common cavitands are based on organic frameworks³ and include notably calixarenes,⁴ cucurbiturils,⁵ cyclotrimeratrylenes,⁶ cyclodextrins,⁷ and resorci-*n*-arenes.⁸ Although these molecules are robust and quite versatile, the tailoring of organic cavitands often requires multistep syntheses that can be tedious and low yielding. One way to obtain cavitands while reducing the synthetic work is using self-assembly processes between organic ligands and metal precursors to generate metallocavitands.⁹ In addition to the ease of synthesis, the presence of metal sites within the cavitand can bring additional properties, such as inducing catalytic activity, facilitating electronic communication, or allowing molecular sensing.

In the past few years, our research group has been interested in the synthesis and properties of conical metallocavitands possessing C₃-symmetry. In a first iteration, the addition of arylboronic acids to Cp^*TaMe_4 afforded tantalum(V) boronate half-sandwich metallocavitands where the trimetallic core is comprised of one $\mu^3\text{-OH}$, one $\mu^2\text{-OH}$, two $\mu^2\text{-O}$, and three $\mu^2\text{-O}_2\text{BR}$ bridges (Scheme 1A).¹⁰ By modifying the nature of the

Scheme 1. (A) $\text{Cp}^*\text{Ta(V)}$ Boronate and (B) CpZr(IV) Carboxylate Clusters



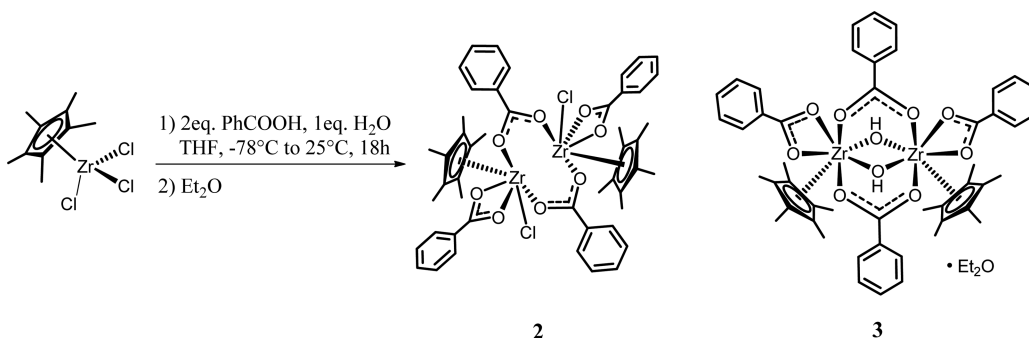
arylboronic acid used in the synthesis, it was possible to obtain extended cavities that could host Lewis bases, such as acetone and THF.^{10c} The guests were shown to be stabilized by hydrogen bonding and by electrostatic interactions, a consequence of the electrophilicity of the boron atoms.^{10b} However, these species did show signs of hydrolysis under basic conditions by cleavage of a B–C bond of the boronate moiety. In order to increase the stability of the metallocavitands, the synthesis of zirconium(IV) carboxylate half-sandwich metallocavitands was carried out.¹¹ Following reported procedures,¹² the addition of carboxylate ligands to Cp_2ZrCl_2 afforded

Received: March 22, 2015

Published: May 20, 2015



Scheme 3. Synthesis of Complexes $(\text{Cp}^*\text{ZrCl}(\kappa^2\text{-OOCPh}))_2(\mu\text{-}\kappa^2\text{-OOCPh})_2$ (**2**) and $[(\text{Cp}^*\text{Zr}(\kappa^2\text{-OOCPh}))_2(\mu\text{-}\kappa^2\text{-OOCPh})_2(\mu^2\text{-OH})_2]\cdot\text{Et}_2\text{O}$ (**3**· Et_2O)



Et_2O (**3**· Et_2O) (Scheme 3). Whereas only a few crystals of **2** were obtained which prevented solution characterization, it was possible to observe that species **3**· Et_2O exhibits lower symmetry in solution, presumably a consequence of the dissociation of the ether molecule and the possible coexistence of more than one species in solution, notably by the presence of several resonances for the phenyl groups between δ 6.96 and 8.17 and by the presence of two Cp^* resonances, each integrating for 15H at 2.03 and 2.06 ppm.

Compound **2** crystallized in the nonclassical central symmetric space group $P2_1/n$. The central Zr atom is coordinated by one Cp^* ligand, one chloride, and two oxygen atoms from one chelating carboxylate group. Two adjacent Zr centers are linked together by two bridging carboxylate groups to form a charge-balanced dimer. Only half of the dimer is located in the asymmetric unit cell, the other part being generated by the inversion operation. As shown in the representation in Figure 2, each metal center of the dimeric

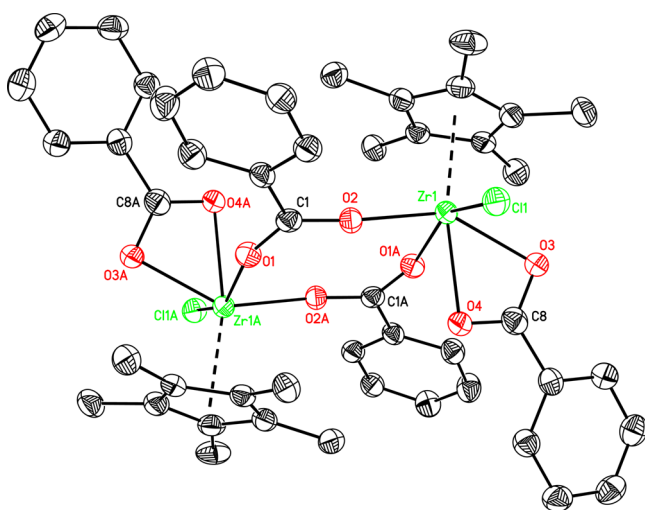


Figure 2. ORTEP drawing of **2** at 50% probability. H atoms are omitted for clarity.

structure consists of a six-coordinated zirconium atom in a heavily distorted octahedron. The $\text{Zr}-\text{O}_3$ and $\text{Zr}-\text{O}_4$ bond lengths for the chelated carboxylate ligand are 2.204(4) and 2.297(4) Å, respectively, whereas the $\text{Zr}-\text{O}_1$ and $\text{Zr}-\text{O}_2$ distances for the bridging ligands are significantly shorter at 2.166(3) and 2.079(3) Å, respectively. The $\text{Zr}-\text{O}$ distances of the chelating ligand are slightly shorter than those observed in the structure of $[\text{Cp}^*_2\text{Zr}(\kappa^1\text{O}-\text{O}_2\text{C}(\text{C}_6\text{H}_4-4\text{-SH}))(\kappa^2\text{-O}_2\text{C}-$

$(\text{C}_6\text{H}_4-4\text{-SH})]^{13b}$ (2.2722(16) to 2.3043(17) Å) and in **1** (2.257(4) and 2.300(4) Å). The $\text{Zr}-\text{Cl}$ distance of 2.4658(15) Å is slightly longer than that observed in the structure of $(\text{Cp})(\text{Cp}^*)\text{ZrCl}_2$ (2.4421(9) Å)¹⁷ but slightly shorter than in **1** (2.4954(17) Å). Replacing one bulky Cp^* by a benzoate moiety greatly reduces the steric environment around the metal center, which can be observed by the short $\text{Zr}-\text{Cp}^*$ centroid distance of 2.211 Å, which is shorter than in **1** (2.259(2) and 2.316(6) Å). The strength of the $\text{Zr}-\text{Cp}^*$ interaction is further exemplified by the three O and the Cl atoms being pushed toward the other vertex of the octahedron ($\text{Zr}-\text{O}_4$), as shown by the cisoid angles ($\text{O}_2-\text{Zr}_1-\text{O}_4$, $\text{O}_1-\text{Zr}_1-\text{O}_4$, $\text{O}_3-\text{Zr}_1-\text{O}_4$, $\text{O}_4-\text{Zr}_1-\text{Cl}_1$) being lower than 90° . The bridging carboxylate group is twisted from the plane of the aromatic ring with a dihedral angle of $22.3(4)^\circ$. The distance between two Zr centers in the dimer is 5.2146(13) Å. The dimers of **2** are packed together into chains along the a axis (Figure S11, Supporting Information) with the chains further aligned together in the $a-c$ plane to form a 3D framework, as shown in Figure S12, Supporting Information.

The structure of compound **3**· Et_2O was refined to the triclinic space group of $P\bar{1}$. Similarly to **2**, two crystallographic independent Zr centers in **3** are coordinated by one Cp^* , two O atoms from one chelating carboxylate group, and two O atoms from two bridging carboxylate moieties (Figure 3). The main difference in **3**· Et_2O when compared to species **2** is that the chlorides are replaced by bridging $\mu_2\text{-OH}$ moieties, forming slightly distorted pentagonal bipyramids rather than octahedral species. As can be observed in the ORTEP structure, the chelated carboxylate groups face each other and can be considered “up”, whereas the bridging carboxylate groups are considered as “down”. One remarkable feature of **3** is the inclusion of one diethyl ether molecule captured between the two carboxylate ligands pointing “up”, forming molecular tweezers. This ether molecule is stabilized mainly by a strong hydrogen bond between the $\mu_2\text{-OH}$ and the O atom in ether, as shown in Figure 3. In order to better understand the nature of the interaction between **3** and Et_2O in play in **3**· Et_2O , the crystallographic data were collected at various temperatures. All of the unit cell parameters have been shown to be sensitive to temperature, indicating its modest flexibility. While the three axes are directly proportional to temperature, the three angles, α , β , and γ , are reversely proportional to temperature (see Table S1, Supporting Information for more details). The structure of **3** at 196 K will be selected for the description of the bond lengths since its refinement is the most reliable.

In **3**· Et_2O the $\text{Zr}-\text{O}$ bond lengths for the chelated carboxylates (Zr_1-O_7 , Zr_1-O_8 , Zr_2-O_9 , $\text{Zr}_2-\text{O}_{10}$) range from

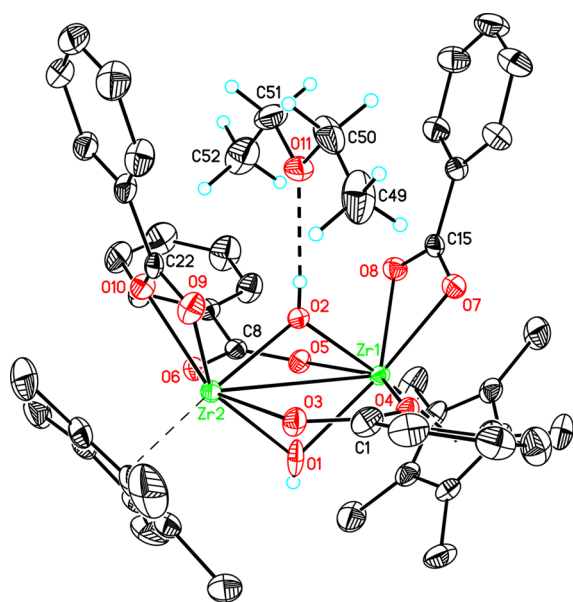


Figure 3. ORTEP drawing of $3 \cdot \text{Et}_2\text{O}$ at 50% probability. H atoms on aromatic rings and Cp^* are omitted for clarity.

2.2763(16) to 2.3052(16) Å, which are comparable to those in **1** and **2**. Because of the presence of two chelating $\mu_2\text{-OH}$ fragments, the distance between Zr_1 and Zr_2 is much shorter than in **2**, at 3.4736(3) Å. The distances between the Zr atoms and the coordinated Cp^* centers are 2.2638(2) and 2.2601(2) Å, respectively. All the equatorial O atoms in the pentagonal bipyramids are pushed toward the vertex of O_2 (for example, $\text{O}_2\text{-Zr}_1\text{-O}_4 = 79.45(6)$, $\text{O}_2\text{-Zr}_1\text{-O}_5 = 78.80(6)$, $\text{O}_2\text{-Zr}_1\text{-O}_1$

$= 73.66(6)$, $\text{O}_2\text{-Zr}_1\text{-O}_8 = 82.24(6)$, $\text{O}_2\text{-Zr}_1\text{-O}_7 = 82.34(6)^\circ$). Interestingly, in the solid state structure, two molecules of **3** are arranged in a mouth-to-mouth fashion to form capsules with two ether molecules captured inside, as shown in Figure 4. The capsules are further linked to form chains along the 101 direction through weak $\pi\text{-}\pi$ interactions between adjacent Cp^* groups. The distance between two Cp^* planes is 3.8695 Å.

At 200 K, the distance between O_2 and the O_{11} atom of diethyl ether is only 2.763 Å with an interaction angle of 176.3° , which would indicate a strong to moderate hydrogen bond.¹⁸ As observed in Figure 5, the distance between the two oxygen atoms increases with temperature (2.742, 2.763, and 2.786 Å at 100, 196, and 296 K, respectively), therefore suggesting the weakening of the hydrogen bond with temperature. Although hydrogen bonding seems to be the primary interaction between **3** and Et_2O , other interactions seem to be present according to the crystallographic data. Indeed, the $\text{C}_{52}\text{-O}_{10}$, $\text{C}_{52}\text{-O}_8$, $\text{C}_{49}\text{-O}_9$, and $\text{C}_{49}\text{-O}_7$ distances (of respectively 3.552, 3.667, 3.502, and 3.673 Å) are short enough to consider possible interactions between the CH bonds of the methyl groups and the π system of the carboxylate moieties pointing “up”. Such interactions would have the effect to decrease the coplanarity between the carboxylate moieties (O-C-O) and the phenyl ring in the phenylcarboxylate ligands, which is observed. Indeed, although the torsion between the aryl group and the OCO moiety is minimal (no twisting), there is folding present at the carboxylic carbon, as observed in Figure 6. The angles between the plane of the aryl group and the plane of the OCO moiety are respectively of 169.3 and 173.3° for the two chelating phenyl carboxylate groups pointing “up”. This folding has also the effect to shorten the distances between the π rings and the C_{51}

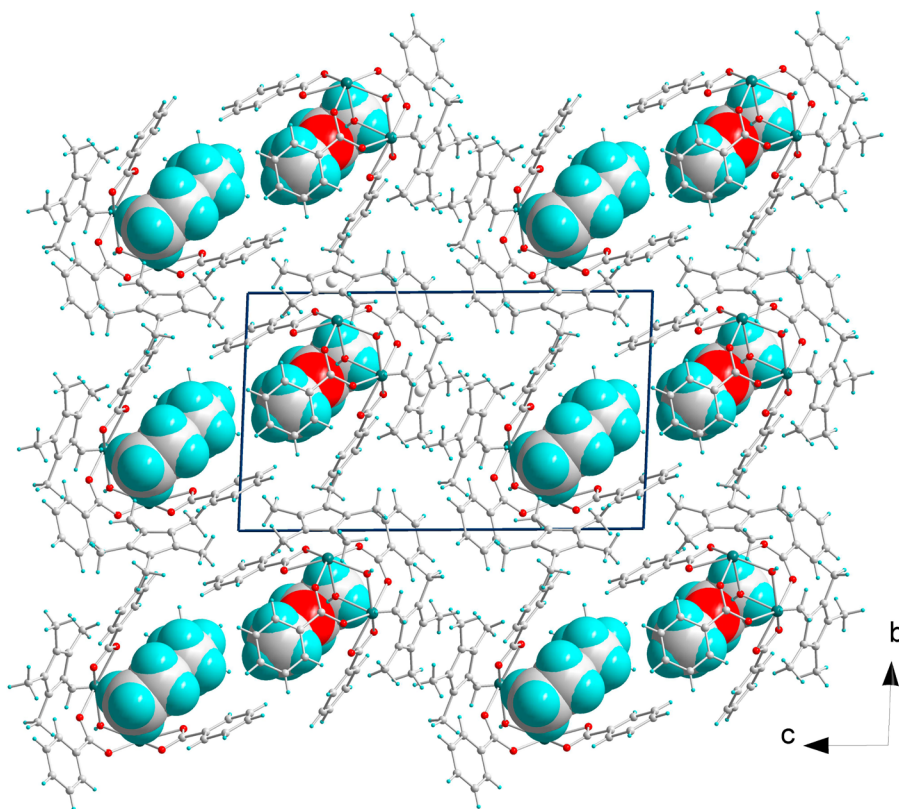


Figure 4. Packing pattern of **3** viewed along the a axis. The guest molecules of diethyl ether are plotted in space filling mode.

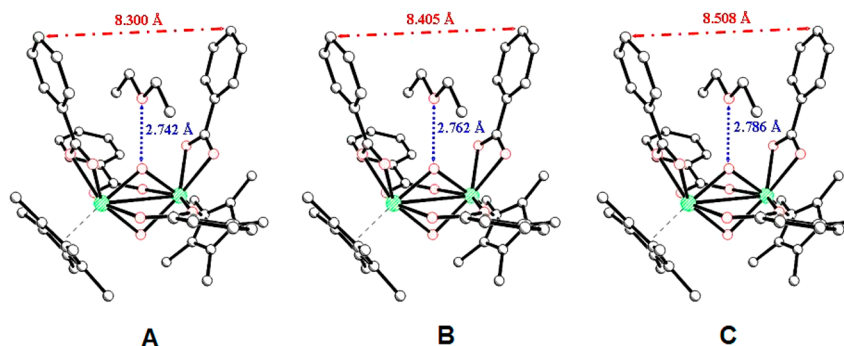


Figure 5. Important structural data for the structure of $3 \cdot \text{Et}_2\text{O}$ at (A) 100 K, (B) 196 K, and (C) 296 K.

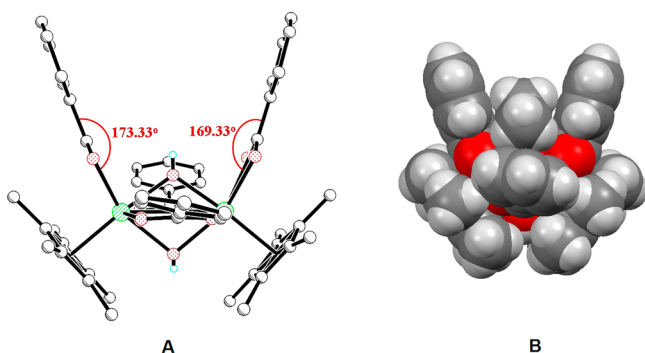


Figure 6. (A) Representation of the folding observed in the phenylcarboxylate ligands and (B) space filling representation of species $3 \cdot \text{Et}_2\text{O}$.

and C50 carbons, suggesting additional interactions. Once again, it is possible to observe that the interaction is stronger at lower temperature, as indicated by the aryl–aryl distance at the extremities of the chelating phenylcarboxylate ligands that is increasing with the temperature (8.300, 8.405, and 8.508 Å at 100, 196, and 296 K, respectively; Figure 5). It is good to note that this folding could be accounted for by packing interactions, and it is difficult to confirm if these secondary interactions are the cause of these structural changes.

Nevertheless, optimized structures of **3** with various solvents, including Et_2O were obtained computationally by calculations based on density functional theory (DFT) using the ωB97XD functional.¹⁹ Since these models are for the gas-phase, the crystal packing should not intervene in the structural parameters observed. As can be observed in Figure 7, significant

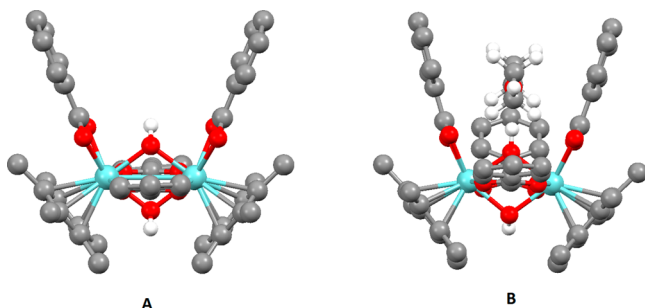
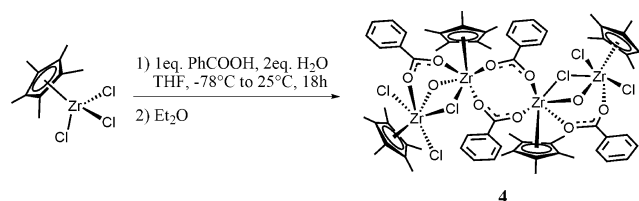


Figure 7. Computationally optimized gas-phase models for (A) **3** and (B) $3 \cdot \text{Et}_2\text{O}$. These results were obtained using the ωB97XD functional and the 6-31G**²⁰ basis set for C, H, and O atoms and the SDD basis set for Zr.²¹

structural changes are observed in the structure of the zirconium cluster between **3** and $3 \cdot \text{Et}_2\text{O}$. In the solvent-free structure, the central hydroxyl group is in an sp^3 environment, with the summation of the angles around the oxygen atom being 336.6° , whereas the summation of the same angles in $3 \cdot \text{Et}_2\text{O}$ is 357.5° . More importantly, there is significant folding between the Zr–OOC plane and the phenyl ring of the chelating phenylcarboxylate (“up”) in the latter model, similarly to what was observed in the crystallographic structure. The average of the folding angles is 173.1° (169.3 and 173.3° in the structure), whereas the same angles have an average value of 178.1° in the solvent-free structure. The two bridging carboxylate moieties (“down”) are more or less parallel to each other in the solvent-free molecule with an angle between the two phenyl rings being close to 180° ; however, one of the phenylcarboxylate moiety is heavily distorted in the $3 \cdot \text{Et}_2\text{O}$ model with folding between the carboxylate plane and the phenyl ring of 126.6° , while the other has a respective angle of 167.4° . DFT supports that **3** is indeed greatly stabilized by interacting with Et_2O since the $\Delta H^\circ_{\text{association}}$ at the gas phase is $-25.3 \text{ kcal}\cdot\text{mol}^{-1}$ ($\Delta G^\circ_{\text{association}}$ of $-9.4 \text{ kcal}\cdot\text{mol}^{-1}$). Interestingly, the association energies for **3** and THF and Me_2O ($\Delta H^\circ_{\text{association}}$ of -23.1 and $-21.1 \text{ kcal}\cdot\text{mol}^{-1}$, respectively) were found to be less important than with Et_2O , even if THF is known to be a better hydrogen bond acceptor, which suggest that the interactions between the CH bonds of the methyl groups and the π system of the carboxylate moieties pointing “up” indeed play a significant role in the stability of the adduct, as proposed above. SMe_2 does not seem to interact with the cavity, which can be expected since sulfur does not form hydrogen bonds as strongly as oxygen. More details are given in the Supporting Information.

In order to see the effect of the water stoichiometry on the products formed, the same reaction was carried out, this time using 2 equiv of water rather than only 1 (Scheme 4). In this situation, a few crystals of the tetrametallic product $[[\text{Cp}^*\text{ZrCl}_2](\mu\text{-Cl})(\mu\text{-OH})(\mu\text{-O}_2\text{CC}_6\text{H}_5)[\text{Cp}^*\text{Zr}]]_2(\mu\text{-O}_2\text{CC}_6\text{H}_5)_2$ (**4**)

Scheme 4. Synthesis of Complex $[[\text{Cp}^*\text{ZrCl}_2](\mu\text{-Cl})(\mu\text{-OH})(\mu\text{-O}_2\text{CC}_6\text{H}_5)[\text{Cp}^*\text{Zr}]]_2(\mu\text{-O}_2\text{CC}_6\text{H}_5)_2$ (**4**)



4

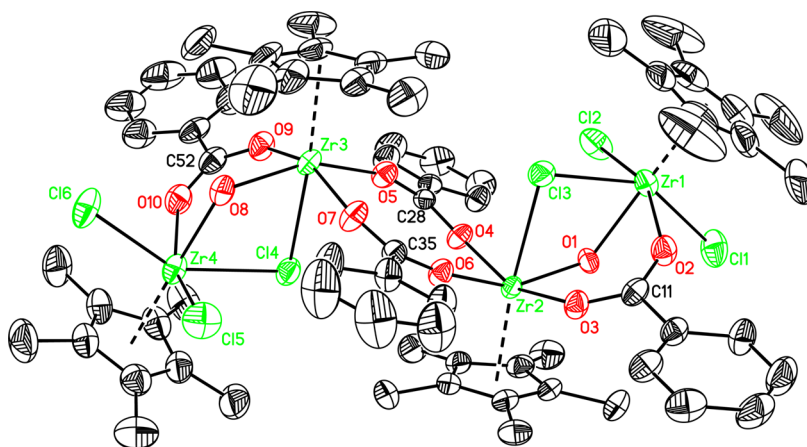


Figure 8. ORTEP drawing of **4** at 50% probability. One of the two independent molecules is shown. H atoms were omitted for clarity.

$\text{O}_2\text{CC}_6\text{H}_5)_2$ (**4**) were observed, enough for a crystallographic study but not for a full characterization, along with a significant amount of amorphous material. Because of the low crystallinity, the hydrogen atoms on the $\mu_2\text{-OH}$ could not be located from the differential Fourier map. It crystallized in the central symmetric space group of $P2_1/c$, with a very long b axis of 38.8446(5) Å. There are two independent molecules present in the unit cell, with one of the two molecules being located on an inversion center, which makes half of that molecule symmetric to the other half. As shown in the ORTEP representation in Figure 8 for one of the two independent molecules, the polynuclear species consists of one Cp^*ZrCl_2 fragment bridging another Cp^*Zr moiety by one chloride, one hydroxide, and one carboxylate group. Two of these bimetallic moieties are bridged together by two carboxylate groups; in one of these two independent molecules only one-half of the molecule moiety is included in the asymmetric unit cell, the other half being generated by the inversion center. All of the zirconium centers are in a pseudo-octahedral environment with the substituents being pushed away from the bulkiest group, the Cp^* . One benzene ring is captured in the structure.

The distances between the centers of the Cp^* planes and the Zr atoms range from 2.2250(5) to 2.2543(4) Å, which are longer than that in **2**, but are comparable to those in **1**. The terminal Zr-Cl bond lengths range from 2.4498(20) to 2.4892(20) Å. Because of the existence of $\mu_2\text{-OH}$, the short Zr-Zr distances range from 3.7665(7) ($\text{Zr}_1\text{-Zr}_2$) to 3.7880(6) ($\text{Zr}_5\text{-Zr}_6$) Å, which are longer than that observed in **3** (3.4736(3) Å). However, the long Zr-Zr distances ($\text{Zr}_2\text{-Zr}_3 = 5.2172(7)$, $\text{Zr}_5\text{-Zr}_5' = 5.2212(6)$ Å) are comparable to that observed in **2** (5.2146(13) Å). The 3D network is illustrated in Figure S17, Supporting Information.

All our attempts to generate a metallocavitand reminiscent to the one observed using the CpZr(IV) moiety failed using phenylcarboxylic acid. However, it is known that simple modifications in the nature of the ligands can affect the structure of the complexes obtained. Using the more acidic 4-bromophenylcarboxylic acid rather than phenylcarboxylic acid in similar conditions, it was possible to observe the formation of ionic species $[(\text{Cp}^*\text{Zr})_3(\kappa_2\text{-O}', \text{O}''\text{C}(\text{C}_6\text{H}_4\text{Br})_3(\mu_3\text{-O})(\mu_2\text{-Cl})_2(\mu_2\text{-OH}))]^+ [\text{Cp}^*\text{ZrCl}_4]^-$ ($[\text{S}]^+ [\text{Cp}^*\text{ZrCl}_4]^-$), which is isostructural to the coveted metallocavitands. According to the charge balance, there should be the presence of one hydroxide in the trimetallic cluster; however, it was not possible to locate the position of the hydrogen atom, making an unambiguous

assignment of the hydroxide group difficult (Figure 9). Close contact between the cation **5** and the $\text{Cp}^*\text{ZrCl}_4^-$ anion mainly

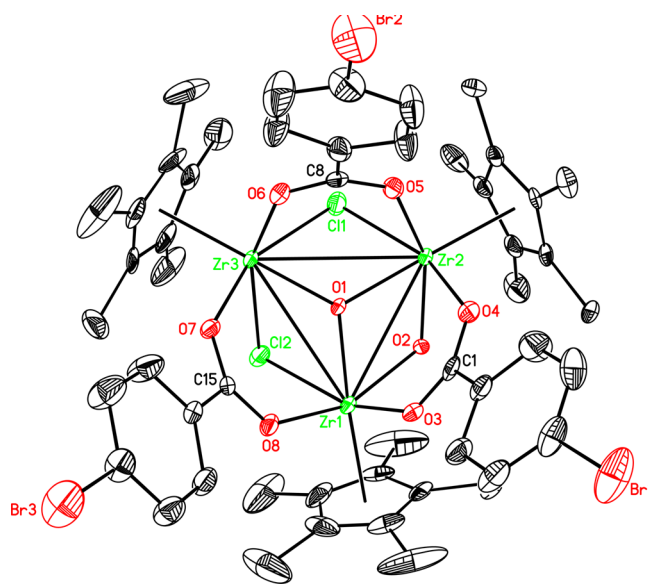


Figure 9. ORTEP drawing of $[\text{5}]^+$ at 50% probability. H atoms are omitted for clarity.

occurs through electrostatic interactions between the bromine in *para* position of the aryl groups and the anion, as represented in Figure S21, Supporting Information. The ion pairs are linked into layers in the $a\text{-}c$ plane, with the layers packed together along the b axis via $\pi\text{-}\pi$ interactions between the Cp^* planes from adjacent **5** units (Figures S19–S20, Supporting Information).

The coordination environment around the metal center in the $[\text{Cp}^*\text{ZrCl}_4]^-$ anion is square pyramidal, with the metal center being 0.8289 Å from the plane composed by the four chloride ligands. The $\text{Cp}^*\text{-Zr}$ distance is relatively short, at 2.1914(10) Å, and the Zr-Cl distances range from 2.453(3) to 2.486(3) Å. However, the main species of interest, the cationic **5** consists of a trimetallic cluster where the three Cp^*Zr moieties are linked together by one $\mu_3\text{-O}$ atom, one $\mu_2\text{-OH}$ group, two $\mu_2\text{-Cl}$ atoms, and three carboxylate groups to form a cluster like in $[(\text{CpZr})_3(\mu\text{-}\kappa_2\text{O}', \text{O}''\text{CR})_3(\mu_3\text{-O})(\mu_2\text{-OH})_3]\text{Cl}$. Because of the special geometry of this cluster, the three

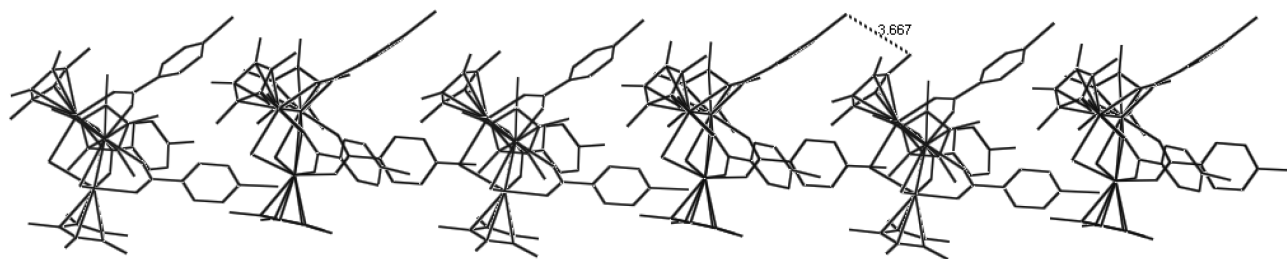


Figure 10. Stacking of species 5.

carboxylate groups form the edge of a bowl, with the metallic cluster forming the bottom.

The Zr-(μ_2 -OH) distances are 2.180(7) and 2.190(6) Å, respectively, which are as expected for a bridging hydroxide group. Indeed, Roesky and co-workers reported that average Zr–O bond lengths for bridging Zr–OH–Zr moieties are around 2.16 Å, whereas the analogous bond lengths for bridging oxide Zr–O–Zr are shorter, varying between 1.945 and 2.106 Å.²² Following the same report, a μ_3 -O can be proposed since the Zr-(μ_3 -O) average bond length in **5** (2.102 Å) is close the expected trend (2.060 and 2.095 Å) for such bridging oxide, whereas bridging hydroxides will have bond lengths between 2.170 and 2.410 Å. As expected by the presence of the two bridging chlorides, **5** does not show a C_3 symmetry but rather possesses a single pseudoplane of symmetry. That can be observed by the presence of two long Zr–Zr distances (3.5557(11) and 3.5806(11) Å) and of one shorter (3.4164(12) Å). The lower symmetry can also be observed in solution where several sets of resonances for the 4-bromobenzoate are observed. The possibility of a further fluxional process in solution is not overlooked since two sharp Cp* are observed at 2.09 and 2.17 ppm, along with one broader resonance at 2.26 ppm when crystals of **5** are put in solution. The Cp*–Zr₃–(μ_3 -O) angle for the metal binding two chlorides is 177.3°, whereas the respective Cp*–Zr–(μ_3 -O) angles for the species binding one chloride are 174.8° on average. Accordingly, the Zr–Cl–Zr angles are 87.5°, whereas the Zr–OH–Zr angle is 102.8°. These results suggest that the more important volume of the chloride anion has the effect to push it away from the metallic core, thereby reducing the Zr–Cl–Zr angles. That steric bulk caused by the chloride has also the effect to give one narrow Zr–(μ_3 -O)–Zr angle of 108.0°, for the metallic centers bridging the hydroxide, and two wider Zr–(μ_3 -O)–Zr angles of 116.1 and 116.9° for the metallic center bridging the chlorides.

The presence of π – π interactions is significant in the crystal lattice. Indeed, it can be observed that two molecules of **5** will interact with each other by interactions through Cp* moieties, as demonstrated by such a distance of 3.72 Å. No inclusion species were observed in the crystal structure of **5**, but the void of the cavity was shown to be filled by stacking of the metallocavitands into each other, as shown in Figure 10. This stacking was notably observed in tantalum metallocavitands previously reported by our research group.^{10a}

CONCLUSION

Although the synthesis of Cp*Zr carboxylate species has been reported previously, the direct synthesis of the zirconium compounds from carboxylic acids and the Cp*ZrCl₃ precursor was never reported, to the best of our knowledge. As expected, the chemistry observed with the more bulky and electron-rich

pentamethylcyclopentadienyl ligand is quite different from the one observed with the Cp-derivatives. The coordination modes of the novel species structurally characterized are very dependent on the reaction conditions, the nature of the solvent, the modification of the phenylcarboxylic acid, and the number of equivalents of water added during the synthesis. Out of the five crystallographic structures that were obtained, two are of notable interest. Species **3** exhibits host–guest characteristics with diethyl ether, which greatly modify the structural parameters of this cluster. The hydrogen bonding and the CH– π contacts were not only observed at the solid-state, but also in the gas-phase models using DFT methods. It was also possible to isolate one of the desired metallocavitands using the 4-Br-phenylcarboxylate ligand, but we have not been successful yet in replacing the bridging chlorides with bridging oxo/hydroxide ligands as it was observed for the CpZr(IV) and Cp*Ta(V) clusters previously reported by our research group.^{10,11} We are currently looking at extending this chemistry and at discovering interesting properties for these metallocavitands notably for host–guest interactions.

EXPERIMENTAL SECTION

General Procedure. Syntheses and subsequent workup of the zirconium clusters were conducted under an atmosphere of nitrogen using standard glovebox techniques. Toluene, DME, THF, and ethyl ether were purified over Na/benzophenone. C₆D₆ was purified by vacuum distillation from a Na/K alloy and CDCl₃ using vacuum transfer techniques under molecular sieves. Cp*ZrCl₃¹⁶ and Cp*₂ZrCl₂²³ were prepared according to literature procedures. Carboxylic acids were purchased from Aldrich and used as received. NMR spectra were recorded on an Agilent Technologies NMR spectrometer at 500 MHz (¹H), 125.758 MHz (¹³C), or a Varian Inova NMR AS400 spectrometer, at 400.0 MHz (¹H), 100.580 MHz (¹³C). ¹H NMR and ¹³C NMR chemical shifts are referenced to residual protons or carbons in deuterated solvent. HRMS data were collected by the Mass Spectrometry Facilities at Laval University with an Agilent 6210 time-of-flight (TOF) LC-MS apparatus equipped with an ESI or APPI ion source (Agilent Technologies, Toronto, Canada).

Synthesis of Cp*₂ZrCl(κ^2 -OOCPh) (1). A solution of benzoic acid (0.112 g, 1.0 mmol) in water (5 mL, pH = 7–8) was added to a solution of Cp*₂ZrCl₂ (0.432 g, 1.0 mmol), and the mixture was stirred at room temperature for 18 h. The organic layer was extracted 3 times (10 mL) with CH₂Cl₂. The organic phases were combined, washed with brine, and dried over MgSO₄. Once filtered, the organic phase was evaporated under a vacuum which yielded a white powder (0.200 mg, 39%). ¹H NMR (400 MHz, CDCl₃) δ 8.11 (d, ³J_{H–H} = 7.2 Hz, 2H), 7.55 (t, ³J_{H–H} = 7.3 Hz, 1H), 7.44 (t, ³J_{H–H} = 7.5 Hz, 2H), 1.88 (s, 30H). ¹³C NMR (101 MHz, CDCl₃) δ 177.6, 133.0, 132.1, 129.4, 128.4, 121.8, 11.7. Exact mass calculated: C₂₇H₃₅ClO₂Zr [M – H₃O]⁺ 535.1557. Found: *m/z* [M – H₃O]⁺: 535.1570.

Synthesis of Cp*ZrCl(κ^2 -OOCPh)₂(μ - κ^2 -OOCPh)₂ (2) and [(Cp*Zr(κ^2 -OOCPh)₂(μ - κ^2 -OOCPh)₂(μ^2 -OH)₂)]·Et₂O (3·Et₂O) (3). A solution of benzoic acid (22 mg, 0.18 mmol) and deionized water (1.6 μ L, 0.09 mmol) in THF (3 mL) was added at –78 °C to a solution of Cp*ZrCl₃ (30 mg, 0.09 mmol) in THF (3 mL). The resulting yellow

solution was stirred at 70 °C for 18 h. The solvent was then removed under reduced pressure to obtain a blue solid. Five milliliters of diethyl ether were added, and a colorless solution was obtained and stirred for 3 h at room temperature until a white precipitate crashed out of the solution. The white precipitate was filtered and washed three times with cold diethyl ether and dried under a vacuum to yield (37 mg, 71% m/m). Crystals of $\text{Cp}^*\text{ZrCl}(\kappa^2\text{-OOCPh})_2(\mu\text{-}\kappa^2\text{-OOCPh})_2$ and $[(\text{Cp}^*\text{Zr}(\kappa^2\text{-OOCPh})_2(\mu\text{-}\kappa^2\text{-OOCPh})_2(\mu^2\text{-OH})_2)\cdot\text{Et}_2\text{O}]$ were obtained from slow evaporation of a solution in diethyl ether and were handpicked for crystallographic analysis. The solution characterization of **2** was not possible because of the lack of material. ^1H RMN $[(\text{Cp}^*\text{Zr}(\kappa^2\text{-OOCPh})_2(\mu\text{-}\kappa^2\text{-OOCPh})_2(\mu^2\text{-OH})_2)\cdot\text{Et}_2\text{O}]$ (C_6D_6): δ 8.17 (br d, $^3J_{\text{H-H}} = 7.4$ Hz, 3H), 8.09 (br d, $^3J_{\text{H-H}} = 7.8$ Hz, 1H), 8.04 (br d, $^3J_{\text{H-H}} = 7.5$ Hz, 2H), 7.97 (br d, $^3J_{\text{H-H}} = 8.1$ Hz, 1H), 7.18 (br s, 1H), 7.16 (br s, 1H), 7.12–7.06 (br m, 6H), 6.99–6.95 (br m, 1H), 2.06 (s, 15H), 2.03 (s, 15H), 1.90 (s, 1H). ^{13}C NMR (101 MHz, C_6D_6) δ 181.5, 133.9, 133.4, 132.5, 129.7, 129.4, 128.9, 128.7, 128.1, 126.3, 123.7, 123.5, 121.7, 65.9 (Et_2O), 15.6 (Et_2O), 12.3, 11.7, 10.7. Exact mass calculated $\text{C}_{52}\text{H}_{62}\text{O}_{11}\text{Zr}_2$ [$\text{M} - \text{Et}_2\text{O} - \text{O}^+$]: 952.1705. Found: m/z [$\text{M} - \text{Et}_2\text{O} - \text{O}^+$]: 952.1633.

Synthesis of $[(\text{Cp}^*\text{ZrCl}_2)(\mu\text{-Cl})(\mu\text{-OH})(\mu\text{-O}_2\text{CC}_6\text{H}_5)(\text{Cp}^*\text{Zr})_2(\mu\text{-O}_2\text{CC}_6\text{H}_5)_2]$ (4**).** A solution of benzoic acid (23 mg, 0.18 mmol) and deionized water (6.9 μL , 0.384 mmol) in THF (5 mL) was added at -78 °C to a solution of Cp^*ZrCl_3 (64 mg, 0.19 mmol) in THF (5 mL). The resulting solution was stirred at room temperature for 18 h. The solvent was then removed under reduced pressure to obtain a blue solid. Ten milliliters of diethyl ether were added, and no precipitate was observed after stirring 48 h at room temperature. Ethyl ether was evaporated, and 5 mL of hexane were added. A white precipitate was observed then filtered. A few crystals were collected from the evaporation of a benzene solution along with degradation material. These crystals were subjected to X-ray analysis.

$[(\text{Cp}^*\text{ZrCl}_4)[(\text{Cp}^*\text{Zr})_3(\kappa^2\text{-O}^-, \text{O}^-(\text{C}_6\text{H}_4\text{Br})_3(\mu_3\text{-O})(\mu_2\text{-Cl})_2(\mu_2\text{-OH}))\text{Cp}^*\text{ZrCl}_4]$ (5**).** A solution of 4-bromobenzoic acid (248 mg, 1.23 mmol) and deionized water (11.1 μL , 0.616 mmol) in THF (10 mL) was added at -78 °C to a solution of Cp^*ZrCl_3 (205 mg, 0.616 mmol) in THF (10 mL). The resulting yellow solution was stirred at 80 °C for 24 h. The solvent was then removed under reduced pressure to obtain a reddish solid. Five milliliters of acetonitrile was added from which a white solid precipitated. The solution was filtered and the filtrate was allowed to crystallize for 1 month. The dried residue was dissolved in benzene from which a yellow precipitate was filtered out. Yellow crystals were obtained from slow evaporation in chloroform and THF (50:50) (79 mg, 21%), ^1H NMR (400 MHz, CDCl_3) δ 7.72 (d, $^3J_{\text{H-H}} = 8.1$ Hz, 3H), 7.62 (d, $^3J_{\text{H-H}} = 8.5$ Hz, 1H), 7.54 (d, $^3J_{\text{H-H}} = 8.1$ Hz, 3H), 7.42 (d, $^3J_{\text{H-H}} = 8.3$ Hz, 2H), 7.27 (d, $^3J_{\text{H-H}} = 8.3$ Hz, 2H), 6.37 (s, 1H), 2.26–2.09 (m, 60H). ^{13}C NMR (101 MHz, CDCl_3) δ 138.0, 132.3, 131.3, 130.2, 128.1, 127.8, 127.6, 126.6, 110.0, 12.4, 12.1. Exact mass calculated: $\text{C}_{51}\text{H}_{58}\text{Br}_3\text{Cl}_2\text{O}_8\text{Zr}_3^+$: 1382.822. Found: m/z [M^+]: 1382.6637.

Crystallographic Data. Single crystals with a suitable size of all compounds were mounted on CryoLoops with Paratone-N and optically aligned on a Bruker SMART APEX-II X-ray diffractometer with 1 K CCD detector using a digital camera. Initial intensity measurements were performed using a fine-focused sealed tube, graphite-monochromated, X-ray source ($\text{Mo K}\alpha$, $\lambda = 0.71073$ Å) at 50 kV and 30 mA. Standard APEX-II²⁴ software package was used for determining the unit cells, generating the data collection strategy, and controlling data collection. SAIN²⁵ was used for data integration including Lorentz and polarization corrections. Semiempirical absorption corrections were applied using SCALE (SADABS).²⁶ The structures of all compounds were solved by direct methods and refined by full-matrix least-squares methods with SHELX-97²⁷ in the SHELXTL6.14 package. As the solvent molecules in some compounds are highly disordered, the SQUEEZE subroutine of the PLATON²⁸ software suit was used to remove the scattering contributions from the highly disordered guest molecules. The resulting new HKL files were used to further refine the structures. All of the H atoms (on C atoms) were generated geometrically and refined in riding mode. Crystallographic information for all obtained phases is summarized in Table S1.

Atomic coordinates and additional structural information are provided in the cif files of the Supporting Information.

Computational Details. Calculations were performed with the GAUSSIAN 09 suite of programs.²⁹ The ωb97xd^{20} functional was used in combination with the 6-31G* basis set for C, H, O, and S atoms²¹ and the SDD basis set for the Zr atom.²² The stationary points were characterized as minima by full vibration frequencies calculations (no imaginary frequency). All geometry optimizations were carried out without any symmetry constraints. All structures with their associated free enthalpy and Gibbs free energies as well as their Cartesian coordinates are fully detailed in the Supporting Information.

■ ASSOCIATED CONTENT

Supporting Information

NMR spectra of species **1–5**, additional crystallographic figures and DFT details are available. The Supporting Information is available free of charge on the ACS Publications website at DOI: 10.1021/acs.inorgchem.5b00634. Crystallographic data have been deposited with CCDC (CCDC No. 1054618 for **1**, CCDC No. 1054619 for **2**, CCDC No. 1054620 for **3** (100 K), CCDC No. 1054621 for **3** (196 K), CCDC No. 1054626 for **3** (296 K), CCDC No. 1054732 for **4**, and CCDC No. 1054625 for **5**). These data can be obtained upon request from the Cambridge Crystallographic Data Centre, 12 Union Road, Cambridge CB2 1EZ, UK, e-mail: deposit@ccdc.cam.ac.uk, or via the Internet at www.ccdc.cam.ac.uk

■ AUTHOR INFORMATION

Corresponding Authors

* (F.-G.F.) E-mail: frederic.fontaine@chm.ulaval.ca.

* (J.-F.M.) E-mail: jean-francois.morin@chm.ulaval.ca.

Notes

The authors declare no competing financial interest.

■ ACKNOWLEDGMENTS

We are grateful to FQRNT (Projet de recherche en équipe - Québec) and CFI (Canada), CCVC (Québec), and CQMF (Québec) for financial support. M.-A.L. is grateful to the NSERC for a scholarship. We acknowledge the help of Pierre Audet with the HR-MS experiments.

■ REFERENCES

- (1) (a) Mahon, C. S.; Fulton, D. A. *Nat. Chem.* **2014**, *6*, 665–672. (b) Pinalli, R.; Dalcanele, E. *Acc. Chem. Res.* **2013**, *46*, 399–411. (c) Uhlenheuer, D. A.; Petkau, K.; Brunsveld, L. *Chem. Soc. Rev.* **2010**, *39*, 2817–2826. (d) Huerta, E.; Metselaar, G. A.; Fragoso, A.; Santos, E.; Bo, C.; de Mendoza, J. *Angew. Chem., Int. Ed.* **2007**, *46*, 202–205. (e) Eckert, J.-F.; Byrne, D.; Nicoud, J.-F.; Oswald, L.; Nierengarten, J.-F.; Numata, M.; Ikeda, A.; Shinkai, S.; Armaroli, N. *New J. Chem.* **2000**, *24*, 749–758. (f) Lehn, J.-M. *Angew. Chem., Int. Ed. Engl.* **1990**, *29*, 1304–1319.
- (2) (a) Leenders, S. H. A. M.; Gramage-Doria, R.; de Bruin, B.; Reek, J. N. H. *Chem. Soc. Rev.* **2015**, *44*, 433–448. (b) Leigh, D. A.; Marcos, V.; Wilson, M. R. *ACS Catal.* **2014**, *4*, 4490–4497. (c) Ballester, P.; Vidal-Ferran, A.; van Leeuwen, P. W. N. M. *Adv. Catal.* **2011**, *54*, 63–126. (d) Hooley, R. J.; Rebek, J., Jr. *Chem. Biol.* **2009**, *16*, 255–264. (e) Pinacho Crisóstomo, F. R.; Lledó, A.; Shenoy, S. R.; Iwasawa, T.; Rebek, J., Jr. *J. Am. Chem. Soc.* **2009**, *131*, 7402–7410.
- (3) (a) Higler, I.; Timmerman, P.; Verboom, W.; Reinhoudt, D. N. *Eur. J. Org. Chem.* **1998**, 2689–2702. (b) Cram, D. J. *Science* **1983**, *219*, 1177–1783.
- (4) (a) Redshaw, C. *Coord. Chem. Rev.* **2003**, *244*, 45–70. (b) Matthews, S. E.; Beer, P. D. *Supramol. Chem.* **2005**, *17*, 411–435.
- (5) (a) Pemberton, B. C.; Raghunathan, R.; Volla, S.; Sivaguru, J. *Chem.—Eur. J.* **2012**, *18*, 12178–12190. (b) Lee, J. W.; Samal, S.;

- Selvapalam, N.; Kim, H.-J.; Kim, K. *Acc. Chem. Res.* **2003**, *36*, 621–630. (c) Yi, J.-M.; Zhang, Y.-Q.; Cong, H.; Xue, S.-F.; Tao, Z. *J. Mol. Struct.* **2009**, *933*, 112–117.
- (6) (a) Hardie, M. J. *Chem. Soc. Rev.* **2010**, *39*, 516–527. (b) Matsubara, H.; Oguri, S.-y.; Asano, K.; Yamamoto, K. *Chem. Lett.* **1999**, *28*, 431–432.
- (7) (a) Liu, Y.; Chen, Y. *Acc. Chem. Res.* **2006**, *39*, 681–691. (b) Hapiot, F.; Tilloy, S.; Monflier, E. *Chem. Rev.* **2006**, *106*, 767–781. (c) Jeon, W. S.; Moon, K.; Park, S. H.; Chun, H.; Ko, Y. H.; Lee, J. Y.; Lee, E. S.; Samal, S.; Selvapalam, N.; Rekharsky, M. V.; Sindelar, V.; Sobransingh, D.; Inoue, Y.; Kaifer, A. E.; Kim, K. *J. Am. Chem. Soc.* **2005**, *127*, 12984–12989.
- (8) Azov, V. A.; Beeby, A.; Cacciarini, M.; Cheetham, A. G.; Diederich, F.; Frei, M.; Gimzewski, J. K.; Gramlich, V.; Hecht, B.; Jaun, B.; Latychevskaya, T.; Lieb, A.; Lill, Y.; Marotti, F.; Schlegel, A.; Schlittler, R. R.; Skinner, P. J.; Seiler, P.; Yamakoshi, Y. *Adv. Funct. Mater.* **2006**, *16*, 147–156.
- (9) (a) Lenthall, J. T.; Steed, J. W. *Coord. Chem. Rev.* **2007**, *251*, 1747–1760. (b) Frischmann, P. D.; MacLachlan, M. J. *Comments Inorg. Chem.* **2008**, *29*, 26–45. (c) Frischmann, P. D.; MacLachlan, M. J. *Chem. Soc. Rev.* **2013**, *42*, 871–890. (d) Han, Y.-F.; Li, H.; Jin, G.-X. *Chem. Commun.* **2010**, *46*, 6879–6890. (e) Huang, C.-C.; Liu, J.-J.; Chen, Y.; Lin, M.-J. *Chem. Commun.* **2013**, *49*, 11512–11514.
- (10) (a) Garon, C. N.; Daigle, M.; Levesque, I.; Dufour, P.; Iden, H.; Tessier, C.; Maris, T.; Morin, J.-F.; Fontaine, F.-G. *Inorg. Chem.* **2012**, *51*, 10384–10393. (b) Garon, C. N.; Gorelsky, S. I.; Sigouin, O.; Woo, T. K.; Fontaine, F.-G. *Inorg. Chem.* **2009**, *48*, 1699–1710. (c) Sigouin, O.; Garon, C. N.; Delaunais, G.; Yin, X.; Woo, T. K.; Decken, A.; Fontaine, F.-G. *Angew. Chem., Int. Ed.* **2007**, *46*, 4979–4982.
- (11) (a) Iden, H.; Morin, J.-F.; Fontaine, F.-G. *Inorg. Chim. Acta* **2014**, *422*, 235–242. (b) Iden, H.; Bi, W.; Morin, J.-F.; Fontaine, F.-G. *Inorg. Chem.* **2014**, *53*, 2883–2891.
- (12) (a) Zhou, Y.-K.; Chen, H.-M. *Polyhedron* **1990**, *9*, 2689–2691. (b) Zhang, R.-F.; Li, C.-P.; Wang, Q.-F.; Ma, C.-L. *J. Coord. Chem.* **2010**, *63*, 2105–2112. (c) Li, J.; Gao, Z.; Han, L.; Gao, L.; Zhang, C.; Tikkanen, W. J. *Organomet. Chem.* **2009**, *694*, 3444–3451.
- (13) (a) Kuate, A. C. T.; Pinkert, L.; Freytag, M.; Jones, P. G.; Tamm, M. Z. *Anorg. Allg. Chem.* **2013**, *639*, 2386–2389. (b) Helmstedt, U.; Lebedkin, S.; Höcher, T.; Blaurock, S.; Hey-Hawkins, E. *Inorg. Chem.* **2008**, *47*, 5815–5820. (c) Helmstedt, U.; Lönnecke, P.; Reinhold, J.; Hey-Hawkins, E. *Eur. J. Inorg. Chem.* **2006**, *23*, 4922–4930. (d) Pellny, P.-M.; Burlakov, V. V.; Baumann, W.; Spannenberg, A.; Rosenthal, U. *Z. Anorg. Allg. Chem.* **1999**, *625*, 910–918. (e) Shah, S. A. A.; Dorn, H.; Gindl, J.; Noltemeyer, M.; Schmidt, H.-G.; Roesky, H. W. *J. Organomet. Chem.* **1998**, *550*, 1–6. (f) Howard, W. A.; Trnka, T.; Waters, M.; Parkin, G. J. *Organomet. Chem.* **1997**, *528*, 95–121.
- (14) (a) Burlakov, V. V.; Arndt, P.; Baumann, W.; Spannenberg, A.; Rosenthal, U. *Organometallics* **2006**, *25*, 1317–1320. (b) Burlakov, V. V.; Arndt, P.; Baumann, W.; Spannenberg, A.; Rosenthal, U. *Organometallics* **2004**, *23*, 4160–4165. (c) Pellny, P.-M.; Kirchbauer, F. G.; Burlakov, V. V.; Baumann, W.; Spannenberg, A.; Rosenthal, U. *J. Am. Chem. Soc.* **1999**, *121*, 8313–8323. (d) Yasuda, H.; Okamoto, T.; Matsuoka, Y.; Nakamura, A.; Kai, Y.; Kanehisa, N.; Kasai, N. *Organometallics* **1989**, *8*, 1139–1152.
- (15) Li, J.; Gao, Z.; Han, L.; Gao, L.; Zhang, C.; Tikkanen, W. J. *Organomet. Chem.* **2009**, *694*, 3444–3451.
- (16) Blenkins, J.; Hessen, B.; van Bolhuis, F.; Wagner, A. J.; Teuben, J. H. *Organometallics* **1987**, *6*, 459–469.
- (17) Rogers, R. D.; Benning, M. M.; Kurihara, L. K.; Moriarty, K. J.; Rausch, M. D. *J. Organomet. Chem.* **1985**, *293*, 51–60.
- (18) Jeffrey, G. A. *An Introduction to Hydrogen Bonding*; Oxford University Press: Oxford, 1997.
- (19) Chai, J.-D.; Head-Gordon, M. *Phys. Chem. Chem. Phys.* **2008**, *10*, 6615–20.
- (20) (a) Francl, M. M.; Pietro, W. J.; Hehre, W. J.; Binkley, J. S.; Gordon, M. S.; Defrees, D. J.; Pople, J. A. *J. Chem. Phys.* **1982**, *77*, 3654–3665. (b) Hehre, W. J.; Ditchfield, R.; Pople, J. A. *J. Chem. Phys.* **1972**, *56*, 2257–2261.
- (21) Andrae, D.; Heussermann, U.; Dolg, M.; Stoll, H.; Preuss, H. *Theor. Chim. Acta* **1990**, *77*, 123–141.
- (22) Bai, G.; Roesky, H. W.; Li, J.; Labahn, T.; Cimpoesu, F.; Magull, J. *Organometallics* **2003**, *22*, 3034–3038.
- (23) (a) Wolczanski, P. T.; Bercaw, J. E. *Organometallics* **1982**, *1*, 793. (b) Manriquez, J. M.; McAlister, D. R.; Rosenberg, E.; Shiller, A. M.; Williamson, K. L.; Chan, S. I.; Bercaw, J. E. *J. Am. Chem. Soc.* **1978**, *100*, 3078.
- (24) APEX2; Bruker AXS Inc.: Madison, WI, 2007.
- (25) SAINT; Bruker AXS Inc.: Madison, WI, 2007.
- (26) Sheldrick, G. M. SADABS; Bruker AXS Inc.: Madison, WI, 2007.
- (27) Sheldrick, G. M. *Acta Crystallogr., Sect. A* **2008**, *64*, 112–122.
- (28) Spek, A. L. *Acta Crystallogr., Sect. D* **2009**, *65*, 148–155.
- (29) Frisch, M. J.; Trucks, G. W.; Schlegel, H. B.; Scuseria, G. E.; Robb, M. A.; Cheeseman, J. R.; Scalmani, G.; Barone, V.; Mennucci, B.; Petersson, G. et al., *Gaussian 09*, Revision D.01; Gaussian Inc.: Wallingford CT, 2009.